EVIDENT

Real-time Insights into Dendrite-Free Zn-Ion Battery Performance

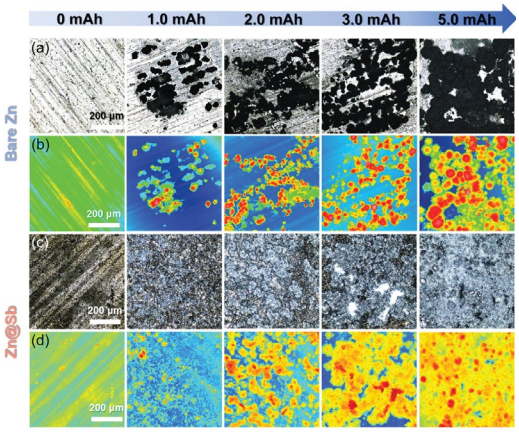

OLYMPUS

WILEY

Contents

Imprint

Boschstr. 12,
69469 Weinheim, Germany
Email: info@wiley-vch.de
Editor: Dr. Christina Poggel

Benefits and Challenges of Zinc-based Batteries

Each battery type offers unique benefits and challenges, and the choice of battery technology is highly dependent on the specific requirements of the research application. Lithium-based batteries lead the market in portable electronics and electric vehicles, while zinc-based and other alternative chemistries are gaining attention for stationary storage and specific niche applications. Continuous research and development are essential to overcome the existing limitations of each battery type and to achieve breakthroughs in energy storage technology. Researchers are encouraged to consider the environmental impact, resource availability, and lifecycle costs of battery technologies in their studies to pave the way for sustainable and practical energy storage solutions.[1]

In the quest for sustainable and reliable energy storage solutions, the development of advanced battery technologies is crucial. Zinc-ion batteries (ZIBs), particularly those employing aqueous electrolytes, are emerging as a compelling alternative to conventional lithium-ion batteries. These batteries offer a promise of safety, cost-effectiveness, and environmental friendliness, thanks to the abundant and non-toxic nature of zinc. However, the full potential of aqueous Zn-ion batteries is yet to be realized, as they grapple with significant challenges that impede their long-term performance and practical application. Chief among these are the uncontrolled growth of zinc dendrites and the concurrent hydrogen evolution reaction at the zinc metal anode, which compromise the battery's reversibility and cycling life.

DENTRITE GROWTH AND CORROSION

Zinc battery longevity and safety are compromised by corrosion, hydrogen gas release, and zinc dendrite formation, which undermine reversibility and lifespan. Hydrogen gas is produced through water decomposition, consuming the electrolyte and forming by-products that pose safety hazards due to rising internal pressure. While optimizing electrolyte composition and introducing additives have been employed to mitigate corrosion, the issue of dendrite growth during charging and discharging cycles persists. These dendrites create additional sites for hydrogen production. Addressing both hydrogen gas evolution and dendrite formation is crucial for the performance and stability of rechargeable zinc-ion batteries (ZIBs). Innovations such as zincophilic sites on anodes have shown promise in promoting uniform zinc deposition, which can help prevent dendrite growth and reduce hydrogen evolution, leading to safer and more reliable ZIBs. [2]

Researchers are exploring various strategies to address these problems, including improving electrolyte compositions, adding protective coatings, and modifying battery components [3]. A stable interface between the battery components is key to enhancing battery life, but creating this interface is complex and often not cost-effective or scalable. Self-assembled molecular layers offer a promising solution for protecting against dendrite formation and side reactions, but their effectiveness in zinc batteries needs further research and validation.

REAL-TIME MONITORING

Real-time monitoring of zinc batteries has been significantly advanced through the use of optical microscopy, especially in the past decade [4]. This technology has proven effective in observing and quantifying the electrochemical processes occurring during energy storage. For zinc-ion batteries, it has been instrumental in pinpointing the precise locations where zinc dendrites begin to form on the anode. Studies have also applied optical microscopy to investigate cathode materials, particularly cobalt oxides, revealing insights into lithium ion movement and the physical changes in particles during charging and discharging cycles.

This eBook delves into the sophisticated realm of rechargeable aqueous ZIBs. It explores cutting-edge strategies and innovations aimed at overcoming the obstacles that currently limit their widespread adoption. By focusing on the development of advanced zinc batteries, the book provides an in-depth look at the latest research and technological advancements that are shaping the future of energy storage in renewable energy systems.

In the work by Godeffroy et al., aqueous Zn–MnO_2 batteries are highlighted as a significant advancement for integrating renewable energy sources like wind and solar power into the electrical grid, owing to their high theoretical capacity and the natural abundance of their materials [5]. Despite these advantages, their practical application is hindered by limited cyclability, likely caused by substantial pH changes during the electrochemical conversion of MnO_2. These pH shifts can lead to the formation and dissolution of zinc hydroxide sulfate (ZHS), which potentially affects the MnO_2 conversion process. Through the application of optical reflectometry, the authors provide *in situ*, real-time visualizations of the MnO_2 electrode during charging and discharging, revealing the pivotal role of solid-phase ZHS in managing these processes. The study demonstrates that while ZHS precipitation can obstruct the discharge of the MnO_2 electrode, it also acts as an essential pH buffer that forestalls the competing oxidation of water during charging, thereby offering new insights into the operational mechanics of aqueous Zn–MnO_2 batteries.

Hong et al. report on the development of a novel strategy to enhance the performance of rechargeable aqueous Zn-ion batteries, which are considered a promising candidate for next-generation energy storage systems [6]. Their study addresses the critical issues of uncontrolled dendrite growth on Zn metal anodes and the often overlooked side hydrogen evolution reaction, which have impeded the practical application of ZIBs. They introduce a uniform and robust metallic Sb protective layer, designed through theoretical calculations and applied to the Zn plate via an *in situ* replacement reaction. This Zn@Sb electrode, in contrast to a bare Zn plate, offers numerous zincophilic sites that facilitate Zn nucleation and creates a more uniform electric field at the Zn anode surface, leading to a dendrite-free Zn deposition. This research presents a simple yet effective approach to concurrently mitigate hydrogen evolution and dendrite growth in ZIBs.

Lastly, a study by Ren et al. addresses the challenges hindering the deployment of Zn metal anodes in aqueous zinc batteries, such as dendritic growth, anode corrosion, and the hydrogen evolution reaction. The researchers introduce a straightforward, energy-efficient, and scalable solution to these problems. They *in situ* generate a hydrophobic self-assembled mercaptan layer with a highly organized structure on the Zn anode's surface. This thin interfacial layer promotes even Zn deposition and protects the anode against water and oxygen-induced corrosion, thereby effectively suppressing dendrite growth and ancillary reactions. The HT-Zn electrode demonstrates remarkable electrochemical stability and reversibility. In practice, the HT-Zn||I2 full cell exhibits a notable increase in specific capacity and maintains ultra-stable cyclability with no capacity decline over 1500 cycles. The success of the SAML approach underscores the significant role of molecular engineering in enhancing the performance of aqueous zinc batteries.

As we navigate through the chapters, the eBook will unravel the multifaceted strategies employed to stabilize zinc anodes, from optimizing electrolyte formulations to designing protective coatings. It will also shed light on the broader implications of these developments for grid-scale applications, particularly in the context of renewable energy integration.

References

[1] *S. Sen, F. H. Richter, Adv. Sci. 2023, 10, 2303985.* https://doi.org/10.1002/advs.202303985

[2] *Y.-P. Deng, R. Liang, G. Jiang, Y. Jiang, A. Yu, Z. Chen, ACS Energy Lett. 2020, 5, 1665.* https://doi.org/10.1021/acsenergylett.0c00502

[3] *Y. Geng, L. Pan, Z. Peng, Z. Sun, H. Lin, C. Mao, L. Wang, L. Dai, H. Liu, K. Pan, X. Wu, Q. Zhang, Z. He, Energy Storage Mater. 2022, 51, 733.* https://doi.org/10.1016/j.ensm.2022.07.017

[4] *B. Chen, H. Zhang, J. Xuan, G. J. Offer, H. Wang, Adv. Mater. Technol. 2020, 5, 2000555.* https://doi.org/10.1002/admt.202000555

[5] *L. Godeffroy, I. Aguilar, J. Médard, D. Larcher, J.-M. Tarascon, F. Kanoufi, Adv. Energy Mater. 2022, 12, 2200722.* https://doi.org/10.1002/aenm.202200722

[6] *L. Hong, L.-Y. Wang, Y. Wang, X. Wu, W. Huang, Y. Zhou, K.-X. Wang, J.-S. Chen, Adv. Sci. 2022, 9, 2104866.* https://doi.org/10.1002/advs.202104866

01 Decoupling the Dynamics of Zinc Hydroxide Sulfate Precipitation/Dissolution in Aqueous Zn–MnO_2 Batteries by Operando Optical Microscopy: A Missing Piece of the Mechanistic Puzzle

Adapted from L. Godeffroy, *et. al.*, 2022

In this study, optical reflectometry is employed to image and quantitatively monitor the in situ charge and discharge processes of MnO_2 electrodes in aqueous Zn–MnO_2 batteries during operation

INTRODUCTION

Designing safe, sustainable batteries is essential for moving from fossil fuels to renewable energy. While Li-ion batteries (LIBs) are common, they're not ideal for grid-scale use. Aqueous Zn–MnO_2 batteries offer a better alternative because of the abundance of Zn and Mn and the safety of their aqueous electrolytes compared to LIBs' flammable ones [1,2].

Figure 1a shows a typical charge–discharge cycle of a Zn–MnO_2 battery, with two plateaus linked to Zn^{2+} and H^+ insertion/extraction, and MnO_2 electrodissolution/electrodeposition. Zinc hydroxides, such as $Zn_4(OH)_6SO_4{\cdot}xH_2O$ (ZHS), may precipitate during MnO_2 electrodissolution but don't always form crystals, complicating mechanistic analysis and limiting the use of spectroscopic techniques.

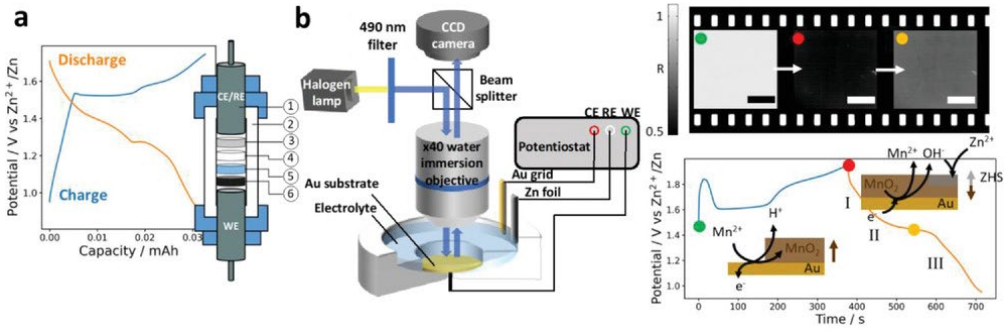

Figure 1. a) Galvanostatic charge–discharge cycle obtained in a two-electrode Swagelok cell. b) Scheme of the operando optical reflectometry setup used to probe MnO_2 conversion on an Au current collector during CV or galvanostatic charge–discharge. Reflectivity images taken at different stages of a galvanostatic charge–discharge cycle, electrolyte: ZHS-saturated 2×10^{-3} M MnSO4 + 2 M $ZnSO_4$, scale bars: 20 µm, and schematic illustration of the material deposition mechanism optically probed during the experiment.

ZHS likely plays a crucial role during charging, as electrolyte acidification from MnO_2 electrodeposition should lead to ZHS dissolution. A promising optical microscopy application developed over the last decade enables imaging and quantification of in situ/operando electrochemical processes in energy storage [3]. In this study, optical reflectometry is employed to monitor the operando preparation of the MnO_2 electrode in an aqueous Zn– MnO_2 battery and its performance in subsequent charge–discharge cycles.

RESULTS

This study, as shown in Figure 1b, involves optically imaging the positive current collector (Au) during the initial MnO_2 electrodeposition from Mn^{2+} in the electrolyte and subsequent charge–discharge cycles. Figure 1b presents a typical galvanostatic charge–discharge cycle under optical monitoring in a 2×10^{-3} M $MnSO_4$-containing electrolyte. Optical images of the electrode surface are continuously acquired (0.5 frames per second) and converted into reflectivity (R) images, representing the relative variation in optical contrast. Figure 1b shows typical reflectivity images at different states of (dis)charge, providing dynamic measurement of local reflectivity (R) during the charge–discharge process.

During charging, the electrode darkens as an MnO_2 film forms, reducing reflectivity. During discharging, the electrode brightens, indicating MnO_2 electrodissolution rather than other conversion processes. By monitoring R, the accumulation/removal of material on the electrode can be tracked. A qualitative analysis of the optical images is initially proposed during cyclic voltammetry (CV) experiments.

In CV analysis, two electrolytes are compared: a typical electrolyte for galvanostatic cycling in a Swagelok cell, diluted in Mn^{2+} (2×10^{-3} M $MnSO_4$ + 2 M $ZnSO_4$, pH ≈ 3.8), and a ZHS-saturated solution (2×10^{-3} M $MnSO_4$ + 2 M $ZnSO_4$, pH ≈ 5.2). Optical images of the Au current collector are recorded and converted into reflectivity images. For thin MnO_2 layers deposited from the $MnSO_4$ electrolyte, the reflectivity of the Au substrate decreases proportionally with the MnO_2 layer thickness.

The reflectivity images are generally homogeneous, as shown in Figure 1b, indicating uniform transformation of the Au surface within the 0.5 µm optical resolution, suggesting non-dendritic MnO_2 growth. Average reflectivity values (over ≈ 1000 µm²) are considered.

During the first forward (oxidation) scan, the Au reflectivity decreases, coinciding with an oxidation peak in the CVs, confirming Mn^{2+} oxidation and Mn-oxide deposition on the Au electrode. During discharge (reverse scan), two reduction peaks are observed in the unsaturated electrolyte. In the ZHS-saturated electrolyte, peak I decreases in intensity (and charge q) in favor of peak II, with a shoulder (III) appearing at 1.3 V, consistent with galvanostatic discharge observations (Figure 1b). Peak I is likely associated with MnO_2 reduction in an acidic environment [4], with its effect reduced by ZHS saturation.

Reflectivity changes during the reverse scan do not fully align with charge evolution, except near the end ($t > 400$ s) in the unsaturated electrolyte, indicating that discharge dynamics (electron injection) are not fully synchronized with MnO_2 dissolution. The better alignment in the unsaturated electrolyte at the end of discharge suggests that the overall process involves MnO_2 dissolving into soluble Mn^{2+}. Reflectivity nearly returns to its original value, and the charge to zero, indicating almost complete dissolution of the MnO_2 deposited during the forward scan.

ZHS PARTICLE-COATED ELECTRODE

Figure 2a shows an optical image of the Au electrode coated with ZHS microparticles, recorded at open circuit in the ZHS-saturated electrolyte. Several micrometric ZHS crystals appear as dark-contrasted features, with the smallest visible features around 0.5 µm. The electrode then undergoes three galvanostatic charge–discharge cycles while being optically monitored operando. These optical images are converted into reflectivity images for the first charge-discharge cycle. To highlight local electrodeposition phenomena, a local MnO_2 thickness, ∂_{MnO2}, relative to a background thickness $\partial_{MnO2,bg}$, is evaluated. Figure 2b provides a map of this relative MnO_2 thickness across the entire imaged region at t = 287 s, while Figure 2c shows a zoomed-in view over a specific particle at different charging times. Unlike in the CV study (without ZHS particles), MnO_2 deposition is not uniform across the Au electrode surface. Overlaying the image of the original ZHS particles reveals that regions surrounding the ZHS particles have higher deposition ($\partial_{MnO2} - \partial_{MnO2,bg} > 0$).

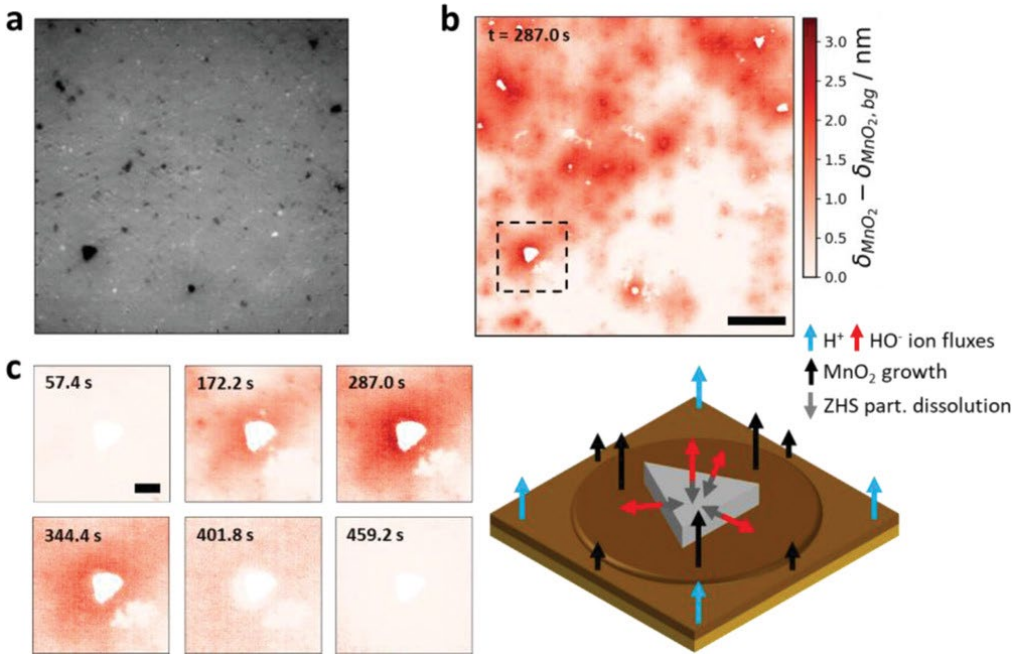

Figure 2. *a) Background subtracted optical reflectometry image of the Au cathode coated with ZHS particles (dark-contrasted features). b) Reflectivity image converted into relative* MnO_2 *thickness,* $\partial_{MnO2} - \partial_{MnO2,bg}$*. The particles detected in a) are masked to highlight that they are surrounded by regions of thicker* MnO_2 *deposits. Scale bar: 50 µm. c) Sequential relative* MnO_2 *thickness images showing the expansion of the excess deposition region around a ZHS particle (zoom inside the dashed region of interest in b)) and schematic mechanistic explanation. Scale bar: 10 µm.*

CONCLUSION

The study used optical reflectometry to examine charge-transfer processes in aqueous Zn–MnO_2 batteries. Findings indicate that MnO_2 electrodeposition and electrodissolution are primary charge storage mechanisms, with ZHS precipitation occurring during discharge. The poor correlation between charge and mass changes may stem from kinetic delays in MnO_2 reduction and material removal. Adjusting ZHS crystallization could eliminate one discharge plateau, aiding battery commercialization. The role of ZHS during charging was also explored, revealing that MnO_2 deposition is tied to ZHS dissolution, which acts as a pH buffer. This work clarifies the origins of charge plateaus and suggests ways to boost Zn–MnO_2 battery capacity.

EXPERIMENTAL SECTION

Operando optical reflectometry was performed using a standard Olympus microscope with a C-mount adapter (U-CMAD3), a 40× water immersion objective (LUMPlanFL N 40×/0.80 W, Olympus), and a CCD camera. As shown in Figure 1b, the substrate is top-illuminated through the objective, with the reflected light collected through the same lens. The substrate tilt is adjusted with a Mirau objective for normal incidence before each experiment. This setup enables 3D spatiotemporal imaging with sub-micrometer lateral and sub-nanometer vertical resolution. Image processing is performed using custom routines.

Electrochemical measurements were conducted with a CHI760e potentiostat (CH Instruments), manually synchronized with the camera. Au-coated Si wafers served as the reflective substrate and working electrode, an Au grid as the counter electrode, and Zn foil as the reference electrode.

References

[1] *Konarov, A. et al. (2018). Present and Future Perspective on Electrode Materials for Rechargeable Zinc-Ion Batteries. ACS Energy Letters.* https://doi.org/10.1021/acsenergylett.8b01552.

[2] *Chen, D. et al. (2021). Recent advances in energy storage mechanism of aqueous zinc-ion batteries. Journal of Energy Chemistry.* https://doi.org/10.1016/j.jechem.2020.06.016.

[3] *Chen, B. et al. (2020). Seeing is Believing: In Situ/Operando Optical Microscopy for Probing Electrochemical Energy Systems. Advanced Materials Technologies.* https://doi.org/10.1002/admt.202000555.

[4] *Rogulski, Z. et al. (2003). Electrochemical behavior of manganese dioxide on a gold electrode. Journal of Electroanalytical Chemistry.* https://doi.org/10.1016/S0022-0728(03)00045-7.

02 Toward Hydrogen-Free and Dendrite-Free Aqueous Zinc Batteries: Formation of Zincophilic Protective Layer on Zn Anodes

Adapted from L. Hong, *et. al.*, 2022

This work provides a facile and effective strategy to suppress hydrogen evolution reaction and dendrite growth in rechargeable aqueous Zn-ion batteries (ZIBs).

INTRODUCTION

Metallic Zn anodes are promising for aqueous batteries due to their safety, low cost, high capacity, and moderate redox potential [1–3]. However, they suffer from hydrogen evolution and Zn dendrite growth, reducing battery life and safety. Hydrogen evolution forms by-products, increasing contact surface area and internal pressure, and posing safety risks. Despite various strategies, uncontrolled dendrite growth remains a challenge, as it accelerates hydrogen evolution by creating more reaction sites. Introducing zincophilic sites can enhance Zn deposition uniformity by improving Zn^{2+} ion interaction and reducing nucleation energy [4,5]. Guided by density functional theory (DFT) calculations, a robust Sb protective layer was prepared on Zn plates via in situ replacement with Sb^{3+}.

RESULTS

DFT calculations show that a thin Sb layer with zincophilic and weak hydrogen adsorption sites can inhibit Zn dendrite growth and hydrogen evolution. It was found that Sb coating on Zn anodes enhances wettability, reducing the contact angle from 98.1° to 58.0°, promoting uniform electrolyte dispersion. It increases surface free energy from 34.7 to 63.9 mN m^{-1}, aiding even Zn^{2+} ion distribution and smooth deposition. Zn@Sb anodes also have lower overpotentials, with nucleation and plateau values reduced to 39.6 and 25.4 mV, compared to 142.2 and 44.3 mV for bare Zn, indicating better interfacial interaction and lower nucleation energy barrier.

The morphology evolution of Zn deposition on bare Zn and Zn@Sb was studied using confocal laser scanning microscopy (CLSM) with loading capacities from 1.0 to 5.0 mAh cm^{-2}. On bare Zn, large particle-shaped Zn dendrites appear even at 1.0 mAh cm^{-2} as a result of limited nucleation sites and poor wettability, leading to uneven Zn deposition (Figure 1a,b). At 5.0 mAh cm^{-2}, large Zn protrusions over 90 μm high cover the surface, risking battery failure caused by separator puncture. In contrast, Zn@Sb shows homogeneous Zn deposits at 1.0 mAh cm^{-2} owing to increased wettability and abundant zincophilic sites, resulting in film-like deposition. At 5.0 mAh cm^{-2}, Zn@Sb forms a flat, dense layer with heights under 43 μm (Figure 1c,d).

Finite element simulation revealed that poor Zn affinity on bare Zn causes random Zn^{2+} ion deposition and irregular protuberances, enhancing local electric field intensity and promoting dendrite formation (Figure 1e). The Sb layer reduces the surface electric field intensity from 256.3 to 130.6 V m^{-1}, creating a uniform field that ensures even Zn^{2+} ion distribution and dendrite-free Zn plating (Figure 1f).

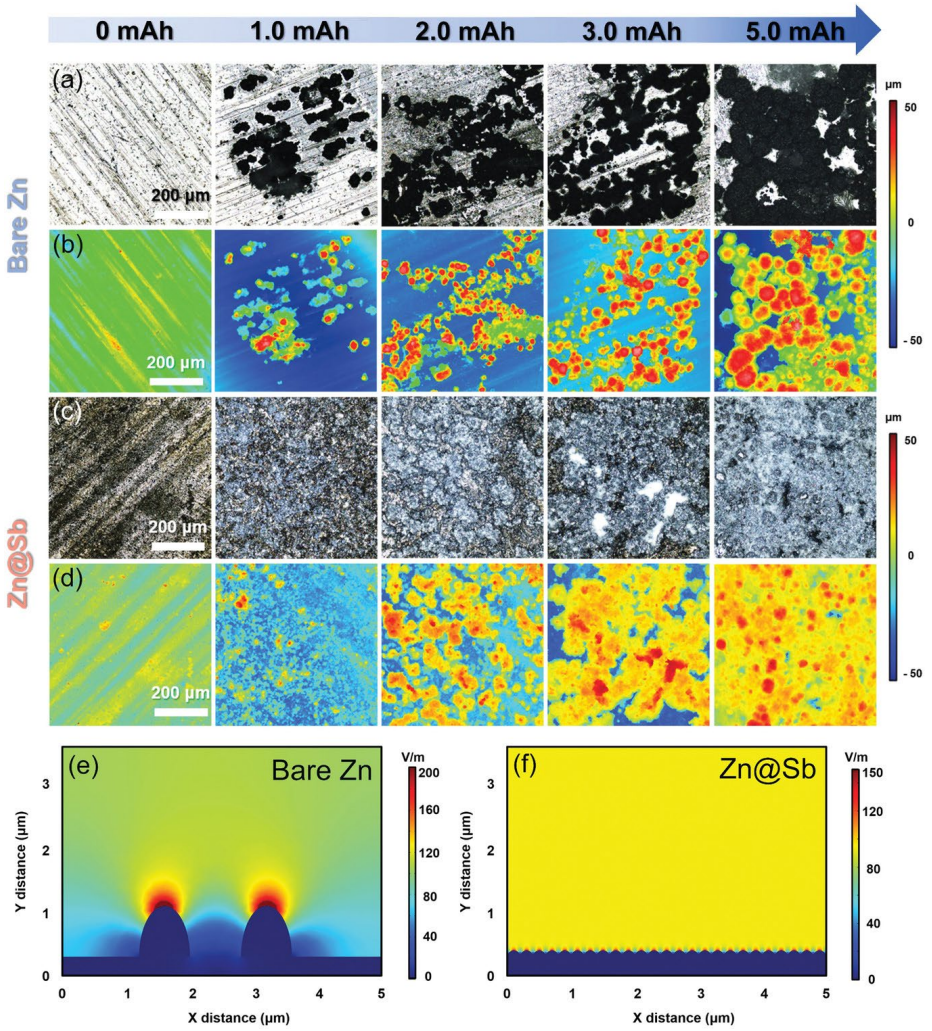

Figure 1. *(a,c) CLSM optical images and (b,d) corresponding height images of Zn deposition at a current density of 0.5 mA cm^{-2} with different capacities on bare Zn and Zn@Sb. Simulated electric field distributions on (e) bare Zn and (f) Zn@Sb.*

The Zn@Sb anode outperforms bare Zn with a longer lifespan and lower voltage hysteresis owing to even Zn deposition. At 1.0 mA cm^{-2} for 1.0 mAh cm^{-2}, Zn@Sb lasts over 800 hours (≈26 mV polarization), while bare Zn fails after 74 hours. At 3.0 mA cm^{-2}, Zn@Sb cycles stably for 1000 hours (≈34 mV hysteresis) and over 900 hours at 5.0 mA cm^{-2}, exceeding many Zn anodes.

Cyclic voltammetry shows Zn@Sb has better plating/stripping kinetics, larger peak area, and higher current intensity than bare Zn, with over 97.7% Coulombic efficiency. Electrochemical impedance spectroscopy reveals much lower charge-transfer resistance (40.1 Ω vs. 704.8 Ω for bare Zn), confirming faster Zn^{2+} transfer. Zn@Sb also maintains lower voltage hysteresis and stable performance across various current densities.

In Zn||MnO_2 full cells, Zn@Sb||MnO_2 outperforms Zn||MnO_2 with higher current intensity, lower voltage polarization, and enhanced reactivity. At 0.5 C, Zn@Sb||MnO_2 delivers 276 mAh g^{-1} vs. 155 mAh g^{-1} for Zn||MnO_2. After 500 cycles at 2 C, Zn@Sb||MnO_2 retains 160 mAh g^{-1} (75.5%), compared to 27 mAh g^{-1} for Zn||MnO_2, demonstrating improved cycling stability by reducing dendrite growth and hydrogen evolution.

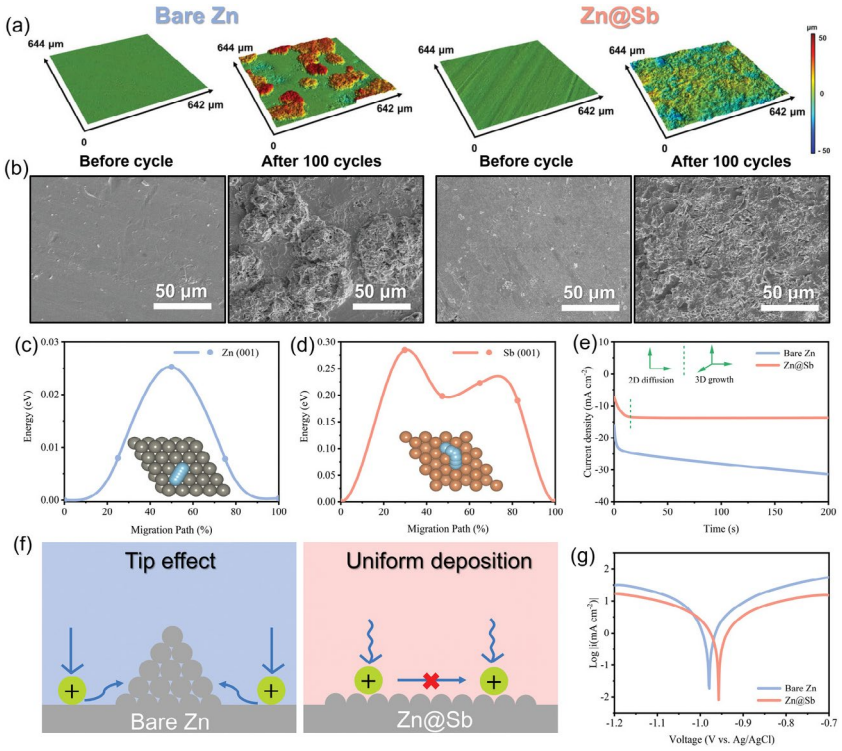

Figure 2. *a) CLSM 3D height images and b) SEM images of bare Zn and Zn@Sb before cycling and after 100 cycles at 1.0 mA cm^{-2} with the capacity of 1.0 mAh cm^{-2}. The calculated migration energy barriers of Zn^{2+} ions along c) Zn (001) and d) Sb (001) surface and corresponding migration pathways (insets). e) Chronoamperograms (CAs) of bare Zn and Zn@Sb at a −150 mV overpotential. f) Schematics of the Zn^{2+} diffusion and reduction processes on bare Zn and Zn@Sb electrodes. g) Corrosion curves of the bare Zn and Zn@Sb anodes.*

CLSM and scanning electron microscopy (Figure 2a,b) show surface changes in bare Zn and Zn@Sb anodes before and after cycling. Before cycling, both anodes have smooth surfaces. After 100 cycles, bare Zn develops island-like dendrites with heights increasing from 5.2 to 102 μm, indicating uncontrolled growth. In contrast, Zn@Sb remains smoother with a height of ≈57 μm, showing more uniform plating. These results confirm that bare Zn develops coarse, irregular dendrites, while Zn@Sb has a more homogeneous surface. This uniformity ensures dendrite-free and reversible cycling.

DFT calculations (Figure 2c,d) show Zn^{2+} diffusion barriers are 0.025 eV on Zn (001) and 0.286 eV on Sb (001), indicating Zn^{2+} migration is hindered on Sb, reducing aggregation. Chronoamperometry (CA) (Figure 2e) shows that bare Zn has increased current density as a result of 2D diffusion and dendrite growth, while Zn@Sb stabilizes quickly owing to constrained 2D diffusion and uniform deposition. Linear polarization tests (Figure 2g) reveal Zn@Sb has a lower corrosion current density (3.90 mA cm^{-2}) compared to bare Zn (7.61 mA cm^{-2}), indicating better corrosion resistance.

CONCLUSION

The low binding energy between Sb and Zn enhances Zn^{2+} ion interaction on Zn@Sb. The Sb layer improves electrolyte wettability, electric field uniformity, and provides zincophilic sites, leading to uniform Zn^{2+} distribution and plating/stripping. The Sb layer also effectively suppresses hydrogen evolution. Consequently, Zn@Sb anodes in symmetric cells show over 1000 hours of stable cycling with low voltage hysteresis, maintaining a dendrite-free and hydrogen-free state. This approach offers a simple, efficient method for high-performance Zn anodes using a thin metal layer.

EXPERIMENTAL SECTION

Sb was coated onto Zn foil anodes by immersing Zn plates into $SbCl_3$ ethanol solution for 5 min. The modified Zn foils were washed with ethanol several times and then dried naturally to obtain the Zn@Sb anodes.

Characterization: the CLSM images were collected on an Olympus OLS5000 microscope. The wettability of electrodes was performed by a contact angle measuring device (DSA30, KRUSS).

Electrochemical Measurements: CR2032-type Zn–Zn symmetric cells were assembled with bare Zn and Zn@Sb, glass fiber separator, and 2.0 m $ZnSO_4$ electrolyte. The cathodes were fabricated with a slurry containing MnO_2, acetylene black and polyvinylidene fluoride (8:1:1). The cathodes and anodes were separated by glass fiber separators. 2.0 m $ZnSO_4$ and 0.1 m $MnSO_4$ aqueous solution was used as electrolyte for all coin cells.

References:

[1] *Ma, L. and Zhi, C. (2021). Zn electrode/electrolyte interfaces of Zn batteries: A mini review. Electrochemistry Communications.* https://doi.org/10.1016/j.elecom.2020.106898.

[2] *Mallick, S. and Raj, C.R. (2021). Aqueous Rechargeable Zn-ion Batteries: Strategies for Improving the Energy Storage Performance. ChemSusChem.* https://doi.org/10.1002/cssc.202100299.

[3] *Zhou, J. et al. (2021). Ultrathin Surface Coating of Nitrogen-Doped Graphene Enables Stable Zinc Anodes for Aqueous Zinc-Ion Batteries. Advanced Materials.* https://doi.org/10.1002/adma.202101649.

[4] *Xie, F. et al. (2021). Mechanism for Zincophilic Sites on Zinc-Metal Anode Hosts in Aqueous Batteries. Advanced Energy Materials.* https://doi.org/10.1002/aenm.202003419.

[5] *Zhang, Y. et al. (2021). Unveiling the Origin of Alloy-Seeded and Nondendritic Growth of Zn for Rechargeable Aqueous Zn Batteries. ACS Energy Letters.* https://doi.org/10.1021/acsenergylett.0c02343.

03 Inhibiting Dendrite Formation and Electrode Corrosion via a Scalable Self-Assembled Mercaptan Layer for Stable Aqueous Zinc Batteries

Adapted from B. Ren, *et. al.*, 2023

This study presents a straightforward, energy-efficient, and scalable method for reducing dendrite growth, anode corrosion, and hydrogen evolution in Zn metal anodes used in aqueous zinc batteries.

INTRODUCTION

While lithium-ion batteries have revolutionized energy storage, their limitations hinder large-scale applications. In the effort to address these issues, aqueous zinc-ion batteries (AZIBs) have gained attention. However, problems such as dendrite growth, anode corrosion, and hydrogen evolution in aqueous electrolytes still limit the use of metallic zinc [1]. Dendrite formation can cause internal short circuits, and side reactions such as Zn corrosion and hydrogen evolution are also problematic [2,3].

Researchers have explored various strategies to tackle these challenges, including optimizing electrolytes, adding additives, designing coatings, modifying separators, and regulating Zn alloys [4]. A stable interface is crucial for battery longevity. Although several effective methods for creating an ideal interface have been proposed [5,6], there is a need for a simple, cost-effective, safe, and scalable solution to improve Zn anode stability and reversibility.

In this work, we developed a highly ordered self-assembled mercaptan layer (SAML) using a facile and scalable method. By applying 1-hexanethiol (HT) to create an ultrathin protective layer on the Zn surface, we leveraged its strong chemical bond with Zn and hydrophobicity to prevent dendrite formation, Zn corrosion, and hydrogen evolution, thereby extending battery life.

RESULTS

A simple solution-soaking method enables the in situ self-assembly of 1-hexanethiol (HT) on Zn. During this process, the sulfhydryl group reacts with Zn to form stable Zn–S bonds, while the alkyl chains align vertically, creating a hydrophobic, ordered layer on the Zn surface (denoted as HT-Zn). This easy and cost-effective method is suitable for large-scale production.

Surface characterization techniques, including Fourier transform infrared spectroscopy, Raman analysis, X-ray photoelectron spectroscopy, and atomic force microscopy, confirm successful self-assembly of HT on Zn through chemical adsorption and Zn–S bond formation. HT-Zn exhibits a smooth, uniform surface compared to the rough bare Zn.

Density functional theory (DFT) calculations reveal that HT molecules preferentially bind to the Zn (100) surface due to its lower adsorption energy, resulting in a stable, high-density SAML.

Galvanostatic cycling tests of Zn||Zn symmetric cells with and without the HT-SAML, conducted at various current densities and areal capacities, show that the HT-Zn||HT-Zn cell remains highly reversible and stable for over 1800 hours,

compared to the bare Zn, which failed after 777 hours owing to short circuits. Additionally, the HT-Zn||HT-Zn cell has a lower overpotential of approximately 63 mV versus 114 mV for the bare Zn||Zn cell.

The rate performance of symmetric cells was compared across current densities from 0.5 to 10.0 mA cm–2. While overpotentials increased with current density in both cells, the HT-Zn||HT-Zn cell consistently showed lower overpotentials than the bare Zn||Zn cell. Coulombic efficiency (CE), assessed using asymmetrical Cu||Zn and Cu||HT-Zn cells at 1.0 mA cm–2 and 0.5 mAh cm–2, indicated that the Cu||HT-Zn cell operated over 1600 cycles with an average CE of 98.5%, reflecting excellent reversibility and Zn utilization. In contrast, the Cu||Zn cell failed after 180 cycles as a result of severe dendrite growth and side reactions.

In situ optical observations of Zn deposition provided direct evidence of HT-SAML's effectiveness. Figure 1a shows that gas bubbles appeared within 20 minutes at 10 mA cm–2 on bare Zn, growing larger over time and signaling severe side reactions. After 40 minutes, the bare Zn surface exhibited small, loose Zn particles that developed into dendrites. Conversely, no bubbles were observed on HT-Zn during 70 minutes of deposition under the same conditions, and the HT-Zn showed uniform, compact Zn deposits (Figure 1b). This demonstrates that the HT-SAML effectively reduces side reactions and promotes orderly Zn deposition, inhibiting dendrite formation.

The stability and durability of the HT protective layer were assessed by X-ray photoelectron spectroscopy (XPS), which confirmed its effective protection of Zn from side reactions and uniform Zn deposition throughout the plating/stripping process.

Electrochemical impedance spectroscopy (EIS) was used to evaluate HT-SAML's anti-corrosion capability. The low-frequency impedance (|Z|0.01) indicates corrosion resistance, with higher values representing better performance [7]. The |Z|0.01 values for bare Zn and HT-Zn were 64.7 $\Omega \cdot cm^2$ and 1.01 × 10^3 $\Omega \cdot cm^2$, respectively, showing that HT-SAML significantly enhances corrosion resistance. Nyquist plots also revealed that HT-Zn's semicircle radius was larger than that of bare Zn, indicating superior corrosion protection and higher charge transfer resistance due to the SAML's hydrophobic nature.

Additionally, potentiodynamic polarization measurements provided corrosion potential (Ecorr) and corrosion current density (i_{corr}) from Tafel plots [8]. HT-Zn had a higher E_{corr} of –0.967 V versus AgCl compared to bare Zn's –0.972 V vs AgCl, and lower icorr values of 1.087 × 10^{-5} A cm^2 versus 1.993 × 10^{-5} A cm^2 for bare Zn. These results indicate that HT-SAML effectively suppresses electrode corrosion.

HT-SAML not only enhances anti-corrosion but also effectively inhibits hydrogen evolution reaction (HER). This is due to the HT layer's ability to repel water molecules, with its hydrophobicity playing a key role.

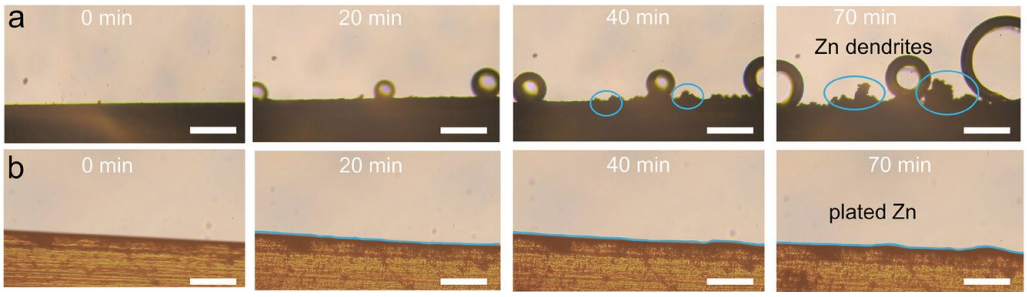

Figure 1. *The suppression of dendrites and side reactions. In situ optical visualization observations of Zn plating behavior of a) bare Zn and b) HT-Zn. Scale bar: 50 μm*

DFT calculations reveal that Zn–H_2O and HT–H_2O binding energies are –21.37 and –11.21 kJ mol^{-1}, respectively, indicating HT-Zn's superior hydrophobicity compared to bare Zn. This hydrophobicity helps prevent water erosion and HER at the electrode. The HT-SAML creates a repulsive barrier against corrosive media and promotes uniform Zn deposition, reducing dendrite formation.

For practical application, HT-Zn anodes were paired with I_2 cathodes (5.0–6.0 mg cm^{-2}) in full cells. The HT-Zn||I_2 cell showed specific capacities of 155, 135, 107, 90, and 78 mAh g^{-1} at 1, 2, 3, 4, and 5 A g^{-1}, respectively. After a slight initial drop, capacity recovered to near 100% CE upon returning to 1 A g^{-1}, demonstrating high reversibility. This performance is attributed to the suppression of dendrite growth and effective corrosion and HER inhibition by the HT-SAML.

To test scalability, a 4 × 4 cm^2 pouch cell with 118 mg areal mass loading was assembled. It operated for 1000 cycles with a CE of ≈99.1% and negligible capacity decay of 0.0098% per cycle, showing excellent stability. The pouch cell's unchanged thickness indicates minimal swelling and gas evolution. Additionally, it successfully powered an LED display, highlighting HT-Zn's practical applicability.

CONCLUSION

In summary, we have demonstrated an innovative and scalable approach to address the inherent issues of dendrite formation, electrode corrosion, and hydrogen evolution in aqueous zinc batteries. Through the in situ formation of a hydrophobic HT-SAML on the Zn anode surface where uniform Zn deposition was facilitated and corrosive water molecules were repelled, the stability and reversibility of the Zn anode were significantly enhanced.

EXPERIMENTAL SECTION

A solution-based self- assembly approach was adopted to fabricate the HT-SAML on Zn surfaces. First, Zn electrodes were polished with an abrasive paper. The polished Zn electrodes were then sequentially cleaned with ethanol and acetone for 15 min, using an ultrasonic cleaner to remove any surface organic pollutants and metallic impurities. After drying under nitrogen gas, the Zn electrodes were immersed in an ethanol solution containing HT (0.1 mol L–1) for 24 h to form HT-SAML. The in situ optical visualization observations were conducted on an optical microscope (Olympus SC180) equipped with an electron multiplying charge-coupled device and monochromator.

References

[1] *Li, C. et al. (2022). Roadmap on the protective strategies of zinc anodes in aqueous electrolyte. Energy Storage Materials.* https://doi.org/10.1016/j.ensm.2021.10.020.

[2] *Xie, F. et al. (2021). Mechanism for Zincophilic Sites on Zinc-Metal Anode Hosts in Aqueous Batteries. Advanced Energy Materials.* https://doi.org/10.1002/aenm.202003419.

[3] *Li, Q. et al. (2022). Towards Understanding the Corrosion Behavior of Zinc-Metal Anode in Aqueous Systems: From Fundamentals to Strategies. Batteries & Supercaps.* https://doi.org/10.1002/batt.202100417.

[4] *Zhong, Y. et al. (2023). Triple-function Hydrated Eutectic Electrolyte for Enhanced Aqueous Zinc Batteries. Angewandte Chemie International Edition.* https://doi.org/10.1002/anie.202310577.

[5] *He, H. et al. (2021). Engineering interfacial layers to enable Zn metal anodes for aqueous zinc-ion batteries. Energy Storage Materials.* https://doi.org/10.1016/j.ensm.2021.09.012.

[6] *Zeng, Z. et al. (2023). Correction: Long cyclic stability of acidic aqueous zinc-ion batteries achieved by atomic layer deposition: the effect of the induced orientation growth of the Zn anode. Nanoscale.* https://doi.org/10.1039/D3NR90009F.

[7] *Ren, B. et al. (2020). Encapsulating polyaniline within porous MIL-101 for high-performance corrosion protection. Journal of Colloid and Interface Science.* https://doi.org/10.1016/j.jcis.2020.06.127.

[8] *Li, W. et al. (2018). Excellent Efficacy of MOF Films for Bronze Artwork Conservation: The Key Role of HKUST-1 Film Nanocontainers in Selectively Positioning and Protecting Inhibitors. ACS Applied Materials & Interfaces.* https://doi.org/10.1021/acsami.8b13602.

About the Sponsor: Seeing is Solving

EVIDENT is Empowering Solutions Through Advanced Visualization

Formerly a wholly owned subsidiary of Olympus Corporation, Evident separated from Olympus in 2022 to become a standalone company.

Built on 100 years of innovative technology and a strong foundation of industry leadership, we are committed to developing new technologies and delivering world-class customer service. At Evident, we are guided by the scientific spirit—innovation and exploration are at the heart of what we do. Committed to making people's lives healthier, safer, and more fulfilling, we support our customers with solutions that solve their challenges and advance their work.

Evident's Micro Imaging Solutions division manufactures a comprehensive range of optical-technology-based systems—including microscopes and objectives, slide scanners, and cell culture solutions—for life science applications like research, education, clinical pathology, hematology, and IVF as well as nondestructive industrial applications.

Our Test and Measurement division manufactures precision nondestructive testing instruments ranging from video borescopes to phased array and eddy current flaw detectors and X-ray fluorescence analyzers for a wide variety of applications, including maintenance, manufacturing, and environment and natural resources. These products are widely used for quality control, inspection, and measurement.

Evident is a steadfast partner that balances expertise in advanced technologies with approachability, so customers know they can bring us their questions, and we'll be ready with innovative technologies and groundbreaking solutions that support and empower them. Evident is hard-working and laser-focused on the needs of its customers to create modern solutions that are globally available. No matter where you work or what your challenge is, Evident can help.

Learn more about who they are.